ACS APPLIED MATERIALS & INTERFACES

RESEARCH ARTICLE

www.acsami.org

Investigation of Photocatalytic Activities over $Bi_2WO_6/ZnWO_4$ Composite under UV Light and Its Photoinduced Charge Transfer Properties

Dongqing He,[†] Lingling Wang,[†,‡] Dandan Xu,[†] Jiali Zhai,[†] Dejun Wang,[†] and Tengfeng Xie[†,*]

[†]State Key Laboratory of Theoretical and Computational Chemistry, College of Chemistry, Jilin University, Changchun 130023, China

[‡]State Key Laboratory of Supramolecular Structure and Materials, College of Chemistry, Jilin University, Changchun 130012, China

Supporting Information

ABSTRACT: $Bi_2WO_6/ZnWO_4$ composite photocatalysts have been successfully synthesized by a facile hydrothermal process. The catalysts were characterized by powder X-ray diffraction (XRD), transmission electron microcopy (TEM), and UV−vis diffuse reflectance spectrum (DRS). The results show that Bi_2WO_6 nanoparticles grow on the primary $ZnWO_4$ nanorods. The $Bi_2WO_6/ZnWO_4$ composites have better UV light photocatalytic activities compared to single $ZnWO_4$ nanorods. Furthermore, the photoinduced charge transfer properties of $Bi_2WO_6/ZnWO_4$ composites were investigated by means of transient photovoltage (TPV) technique in detail. The interconnected interface of $Bi_2WO_6/ZnWO_4$ composites led to the low recombination ratios of photoinduced electron−hole pairs and enhanced photocatalytic activities.

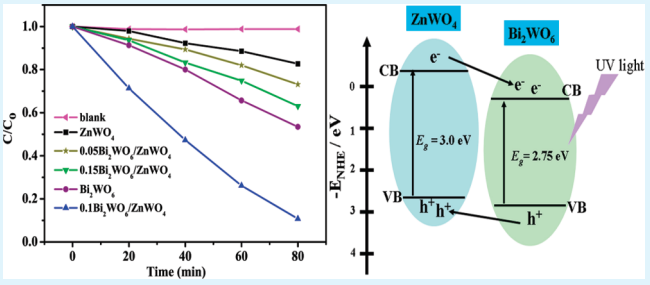

KEYWORDS: $Bi_2WO_6/ZnWO_4$ composite, photoinduced charge transfer, transient photovoltage, photocatalysis

INTRODUCTION

Photocatalytic degradation of organic pollutants by semiconductor photocatalysts has the potential to be a beneficial technology for environmental purification.[1−3] As an important photocatalyst, $ZnWO_4$ has been applied for photocatalytic hydrogen production from water and mineralization of organic pollutants under UV light irradiation.[4−6] However, further research on the improvement of $ZnWO_4$ photocatalytic activities is still indispensable. Many efforts have been made on the improvement of activities, such as morphologies, crystallinity, and ion doping.[6−10] Huang and co-worker found that the doped fluorine ions could cause the distortion of the WO_6 octahedron in a $ZnWO_4$ crystal and enhance the photocatalytic degradation activities to 2.6 times the of rhodamine B (RhB) when the optimal atomic ratio of F/Zn was 0.4.[7] Instead of using a single photocatalyst, coupling of photocatalyst with other semiconductors, metals, or molecules to form junction structures has been found to be significantly benefits to enhance the photocatalytic activities.[11−14] Jang et al. investigated that CdS/TiO_2 composite photocatalyst exhibited a higher hydrogen production rate than that of single CdS nanowires.[15,16] Bi_2WO_6/TiO_2 heterostructure shows enhanced photocatalytic performance over that of TiO_2 due to the higher efficiency of charge carrier separation.[14,17] To date, the composite photocatalyst based on $ZnWO_4$ has not been reported. In this work, we chose Bi_2WO_6 as a functional component for the preparation of $Bi_2WO_6/ZnWO_4$ composite. Bi_2WO_6 has been found as an excellent photocatalyst with a narrow band gap (~2.6 eV).[18] Furthermore, both Bi_2WO_6 and $ZnWO_4$ belong to the tungstate family, and have similar crystalline structures because chains of the tungstate groups WO_6. It can be expected to construct perfect $Bi_2WO_6/ZnWO_4$ composite structure to enhance photocatalytic activity of $ZnWO_4$.

The transient photovoltage (TPV) technique can be applied to analyze the dynamic properties of photoinduced charge carriers,[19] which could provide insight into the transfer behaviors of photoinduced charge carriers in the system, including the generation, separation, and recombination of the photogenerated charges. An outstanding example is Fe_2O_3/TiO_2 heterogeneous photocatalysts reported by Peng and co-workers.[20] In their work, they demonstrated that the formation of the interface between Fe_2O_3 and TiO_2 was pivotal for improving the separation and restraining the recombination of photoinduced electrons and holes, which led to the enhancement of photocatalytic activity.

In this paper, we first successfully prepared $Bi_2WO_6/ZnWO_4$ composite photocatalysts consisting of $ZnWO_4$ nanorods decorated with Bi_2WO_6 nanoparticles. During the degradation of rhodamine B (RhB) under UV light irradiation, the $Bi_2WO_6/ZnWO_4$ composite exhibited much higher photocatalytic activities than that of single $ZnWO_4$ nanorods. The highest efficiency is obtained when $Bi_2WO_6/ZnWO_4$ mole ratio in a solution used for synthesis is 0.1. The TPV measurements suggest that the

Received: May 25, 2011
Accepted: July 11, 2011
Published: July 11, 2011

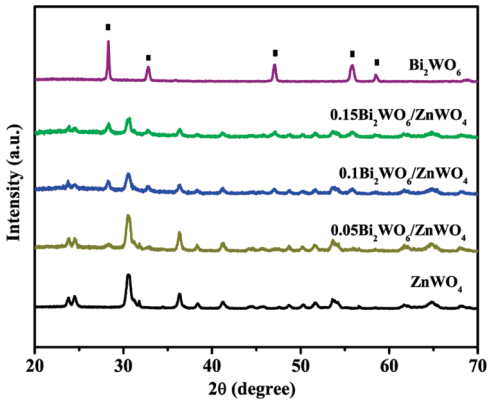

Figure 1. XRD patterns of pure $ZnWO_4$, Bi_2WO_6, and the Bi_2WO_6/$ZnWO_4$ composites with different molar ratios of $ZnWO_4$ vs Bi_2WO_6, respectively.

photoinduced charge transfer properties of Bi_2WO_6/$ZnWO_4$ composite is related to the photocatalytic activities of samples.

EXPERIMENTAL SECTION

Synthesis of $ZnWO_4$ Nanorods. Sodium tungstate dehydrate ($Na_2WO_4 \cdot 2H_2O$, 5 mmol) and Zinc nitrate hexahydrate ($Zn(NO_3)_2 \cdot 6H_2O$, 5 mmol) were added into 30 mL deionized water under stirring at room temperature, based on our previous paper.[21] The pH value of the mixed solution was adjusted to 9.0 using the dilute HCl and NaOH solution (0.5 M). After being vigorously stirred for about 30 min, the solution was loaded into a 50 mL Teflon-lined autoclave. The autoclave was heated at 180 °C for 48 h under autogenous pressure and then cooled to room temperature naturally. The white precipitate was collected and washed with ethanol and distilled water several times. Finally the sample was dried in a vacuum oven at 50 °C for 4 h.

Synthesis of Bi_2WO_6/$ZnWO_4$ Composite Photocatalysts. Bismuth nitrate ($Bi(NO_3)_3 \cdot 5H_2O$) and sodium tungstate dehydrate ($Na_2WO_4 \cdot 2H_2O$), in a molar ratio of 2:1, were dissolved in ethylene glycol (EG) and H_2O, respectively. Then the above solutions were mixed together to form a white suspension and 0.4 mmol of $ZnWO_4$ nanorods (Bi_2WO_6/$ZnWO_4$ molar ratio: 0.05, 0.1, and 0.15) were added into the suspension under vigorously stirring. After stirring for 30 min, the resulting suspension was added into a Teflon-lined autoclave. The autoclave was sealed and heated to 120 °C for 15 h. The precipitate was collected and washed with ethanol and distilled water several times. Then, the sample was dried in a vacuum at 50 °C for 4 h. The composite photocatalysts were marked as 0.05 Bi_2WO_6/$ZnWO_4$, 0.1 Bi_2WO_6/$ZnWO_4$, and 0.15 Bi_2WO_6/$ZnWO_4$. For comparison, the single Bi_2WO_6 sample without $ZnWO_4$ was also prepared via the same solvothermal method.

Characterization. The as-obtained products were characterized by X-ray diffraction (XRD) patterns on a Rigaku D/Max-22550 diffractometer with Cu Kα radiation over the range of $20° \leq 2\theta \leq 70°$. The morphology and microstructure were obtained by a transmission electron microscopy (TEM and HRTEM; TECNAIG^2 FEI company) and a XL 30 ESEM FEG field emission scanning electron microscope (FESEM; FEI Company). UV−vis diffuse reflectance spectra (DRS) were recorded on a UV-3600 (Shimadzu) spectrophotometer.

TPV Measurement. The TPV measurements were carried out by a homemade device described in our previous paper.[20] The samples were excited with a laser radiation pulse (wavelength of 355 nm and pulse width of 5 ns) from a third-harmonic Nd:YAG laser (Polaris II, New Wave Research, Inc.). The TPV signal was recorded by a 500 MHz digital phosphor oscilloscope (TDS 5054, Tektronix). The construct of the photovoltaic cell is a sandwich-like structure of Pt net-sample-ITO. The formation of a TPV signal was determined by the factors of light absorption, transport of excess carriers, structural, and electric characteristics of a semiconducting meterial. The TPV measurements were finished in air atmosphere at room temperature.

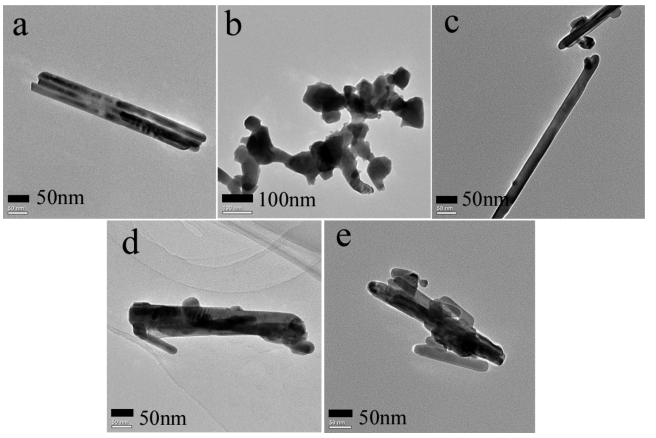

Figure 2. TEM images of the as-obtained samples: (a) $ZnWO_4$, (b) Bi_2WO_6; (c) 0.05 Bi_2WO_6/$ZnWO_4$, (d) 0.1 Bi_2WO_6/$ZnWO_4$, (e) 0.15 Bi_2WO_6/$ZnWO_4$.

Photocatalytic Experimental. The photocatalytic activities of the samples were evaluated by the degradation of the RhB under a 500 W mercury lamp illumination. Powder photocatalyst (20 mg) was dispersed into 20 mL of RhB solution (10 mg/L). Before illumination, the suspensions were vigorously stirred in dark for 1 h to ensure the establishment of an adsorption−desorption equilibrium between the photocatalyst powder and RhB. After that, the solution was exposed to UV light irradiation under magnetic stirring, and 0.8 mL of the suspension was taken from the reaction cell at certain intervals and separated by a centrifugal machine during the process. Finally, the UV−vis spectra of the centrifuged solution were recorded using a Maya2000-Pro spectrometer (Ocean Optics).

RESULTS AND DISCUSSION

Characterization of Composite Photocatalysts. The X-ray diffraction (XRD) of Bi_2WO_6, $ZnWO_4$, and Bi_2WO_6/$ZnWO_4$ composite photocatalysts are shown in Figure 1, respectively. The pure-phase $ZnWO_4$ is a monoclinic structure and the corresponding JCPDS number is 73−0554. When the molar ratio of Bi_2WO_6/$ZnWO_4$ is increased from 0.05 to 0.15, the diffraction peaks of orthorhombic Bi_2WO_6 (JCPDS 39−0256) are intensified gradually, whereas the peak intensities of $ZnWO_4$ decreased. No impurity peak is found in Bi_2WO_6/$ZnWO_4$ composites, suggesting that the composites have a two-phase composition: Bi_2WO_6 and $ZnWO_4$.

Figure 2 shows the TEM images of $ZnWO_4$, Bi_2WO_6, and Bi_2WO_6/$ZnWO_4$ composite photocatalysts, respectively. The pure $ZnWO_4$ synthesized at 180 °C for 48 h possesses the rodlike structure. Meanwhile, the low-magnification FESEM image of pure $ZnWO_4$ is shown Figure S1 in the Supporting Information. It shows that the length of $ZnWO_4$ nanorods is about 500 nm and diameter is about 30 nm. The Bi_2WO_6 can grow into irregular nanoplates structure due to the high intrinsic anisotropic nature.[22] With the increase of the Bi_2WO_6/$ZnWO_4$ molar ratio from 0.05 to 0.15, the concentration of Bi_2WO_6 on $ZnWO_4$ increased, which is in accordance with the XRD results. It is interesting that no individual Bi_2WO_6 nanoparticle in a dispersed

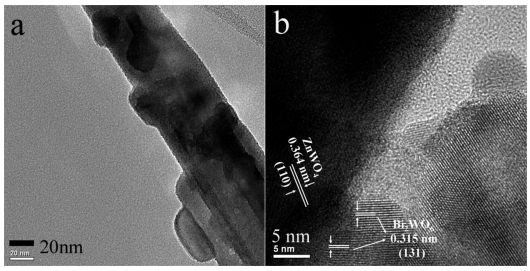

Figure 3. (a) TEM and (b) HRTEM images of the as-obtained sample of 0.1 $Bi_2WO_6/ZnWO_4$.

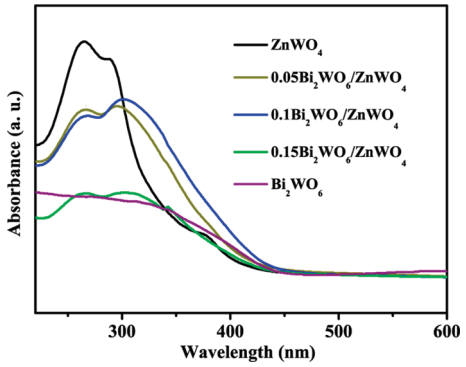

Figure 4. UV−vis diffuse reflectance spectra of $ZnWO_4$, Bi_2WO_6, and $Bi_2WO_6/ZnWO_4$ composites at different molar ratios.

way was found in the solution through ultrasonically treatment for preparation of TEM grids, as shown in Figure S2 in the Supporting Information. The phenomena indicate that the growth of small Bi_2WO_6 nanoparticles tend to attach on the backbone of the $ZnWO_4$.

The HRTEM image of as-obtained $Bi_2WO_6/ZnWO_4$ molar ratio of 0.1 is shown in Figure 3. The low-magnification HRTEM image in Figure 3a shows that $ZnWO_4$ nanorods have a coarse outlayer. The growth of small Bi_2WO_6 nanoparticles attach on the backbone of the $ZnWO_4$. The lattice resolved HRTEM image indicates that the spacing of the lattice is 0.315 and 0.364 nm (as seen in Figure 3b), which is consistent with the spacing of (113) and (110) planes of orthorhombic Bi_2WO_6 and monoclinic $ZnWO_4$, respectively. The high-quality image of the interface between $ZnWO_4$ and Bi_2WO_6 crystal can be observed clearly.

Figure 4 shows the diffuse reflectance spectra of the photocatalysts. The greatly enhancement of the absorption at about 410 nm is due to the band−band transition of $ZnWO_4$.[4] It is also shown that an absorption edge of Bi_2WO_6 photocatalyst is at 450 nm. The spectra of $Bi_2WO_6/ZnWO_4$ composite photocatalysts show the combinations of the two spectra of $ZnWO_4$ nanorods and Bi_2WO_6. From Figure 4, it can be seen that the characteristic absorption peak of $ZnWO_4$ nanorods at 265 and 289 nm. Because the Bi_2WO_6 nanoparticles were coated on the $ZnWO_4$ nanorods, the absorption of 0.05 $Bi_2WO_6/ZnWO_4$ composite shows a red shift from 289 to 297 nm. With the increasing of $Bi_2WO_6/ZnWO_4$ molar ratio, other composites show the red shift from 289 to 304 nm. It is believed that the red shift in the $Bi_2WO_6/ZnWO_4$ composite may be related with the excitons partial leakage into the Bi_2WO_6 matrix.[23] The similar phenomena were reported by Zhang and co-workers. In their

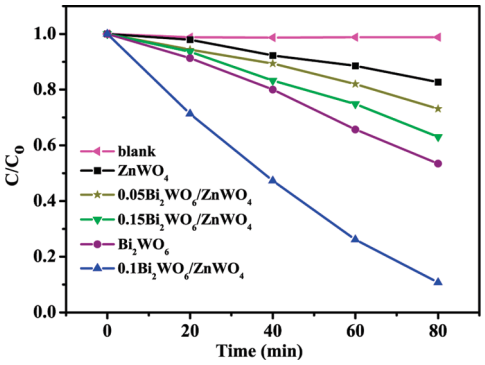

Figure 5. Photocatalytic degradation of RhB (10 mg/L, 20 mL) by different photocatalysts under UV light irradiation, where C is the absorption intensity of RhB at the maximum wavelength of 554 nm irradiated by different time and C_0 is the absorption intensity of RhB after the adsorption−desorption equilibrium on photocatalyst before irradiation. (left-facing triangle) Blank experiment in the solution of RhB; (■) pure $ZnWO_4$; (star) 0.05 $Bi_2WO_6/ZnWO_4$; (▼) 0.15 $Bi_2WO_6/ZnWO_4$; (●) pure Bi_2WO_6; (▲) 0.1 $Bi_2WO_6/ZnWO_4$.

ZnWO−MWO_4 (M = Mn, Fe) core−shell system, the absorption peak for the $ZnWO_4$−MWO_4 (M = Mn, Fe) core−shell nanorods shifts lightly to longer wavelength compared with the bare $ZnWO_4$ nanorods.[24]

Photocatalytic Activity. The degradation of RhB under UV light irradiation was investigated in Figure 5. The blank experiment (without photocatalysts) shows that the degradation of RhB is negligible. The results indicate that the $Bi_2WO_6/ZnWO_4$ composite photocatalysts possess better activities than that of single $ZnWO_4$. As shown in Figure 5, the 0.1 $Bi_2WO_6/ZnWO_4$ sample exhibits much higher photocatalytic activities than those of other samples. With the increasing of the amounts of Bi_2WO_6 nanoparticles, the photocatalytic activities of 0.15 $Bi_2WO_6/ZnWO_4$ reduce. But it still maintains better photocatalytic activities compared to single $ZnWO_4$. In addition, it is shown that the adsorption of RhB from aqueous solution on the photocatalysts in dark $ZnWO_4$, Bi_2WO_6, 0.05 $Bi_2WO_6/ZnWO_4$, 0.1 $Bi_2WO_6/ZnWO_4$, and 0.15 $Bi_2WO_6/ZnWO_4$ are 12, 14, 7, 15, and 12%, respectively. Although the absorption data are similar, their photocatalytic activities of samples are different, implying that the influence of adsorption is ignored in photocatalytic reaction. Therefore, the enhanced photocatalytic activities of composite photocatalysts probably result from the properties of photoinduced charge carries. These properties may be influenced by the structure characteristics of the $Bi_2WO_6/ZnWO_4$ composites. TPV can provide the dynamic information of photoinduced charge carriers in the system, which is a benefit for further understanding the photocatalytic ability of composite photocatalysts.

Figure 6 shows TPV spectrum of as-obtained samples. There are several interesting features: (I) All the TPV signals are positive, which indicates that photoinduced electrons move toward the bulk and photoinduced holes move toward the surface.[25,26] (II) Two peaks at the time shorter than 1×10^{-6} s and the time longer than 1×10^{-4} s can be observed in the TPV response of $Bi_2WO_6/ZnWO_4$ composites, respectively. (III) When the time is shorter than 1×10^{-6} s, the TPV signals arise immediately with the laser pulse. It is a typical behavior for the surface photovoltage in semiconductors where charges carriers are separated by drift in the electric field of the surface space-charge region.[27] The amplitude of

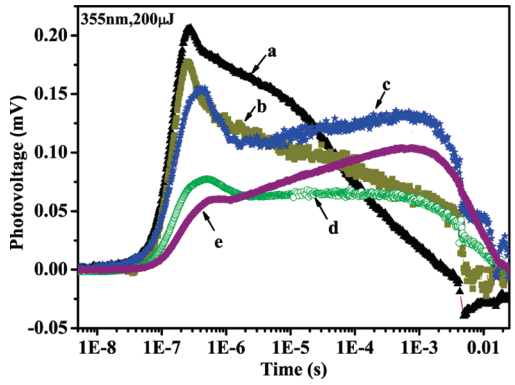

Figure 6. TPV of the samples at different molar ratios of Bi_2WO_6/$ZnWO_4$ composite photocatalysts: (a) $ZnWO_4$, (b) 0.05 Bi_2WO_6/$ZnWO_4$, (c) 0.1 Bi_2WO_6/$ZnWO_4$, (d) 0.15 Bi_2WO_6/$ZnWO_4$, (e) Bi_2WO_6. The wavelength and intensity of the laser pulse are 355 nm and 200 μJ, respectively.

the fast TPV response (at the time shorter than 1×10^{-6} s) decrease with the increasing ratio of Bi_2WO_6 nanoparticles from 0 to 0.15. It demonstrated that Bi_2WO_6 may act as a physical barrier which can absorb most of light. The thickness of Bi_2WO_6 grown on the surface of $ZnWO_4$ nanorods is thickened with the increasing of the molar ratio of Bi_2WO_6/$ZnWO_4$ composites. The areas of $ZnWO_4$ exposed in illumination are decreasing with reducing the chances of $ZnWO_4$ exciting. (IV) Furthermore, an obvious retardation is observed in the TPV of 0.1 Bi_2WO_6/$ZnWO_4$ composite in comparison to that of the bare $ZnWO_4$. It shows that besides the drift of the photoinduced charges at surface, the additional drift at the interface between Bi_2WO_6 and $ZnWO_4$ contributes to the retardation time. The larger retardation time is, the lower recombination rate of electron−hole pairs will be. This means that photoinduced charges will have much time to participate in the photocatalytic reaction before recombination. (V) At time longer than 1×10^{-6} s, the time of TPV maximum of as-obtained samples is strongly retarded, which is typical for diffusion photovoltage.[25,26] As shown in Figure 6, Bi_2WO_6/$ZnWO_4$ composite photocatalysts with molar ratio of 0.1 and 0.15 (curves 6c and 6d) possess the retarded TPV peak corresponding to diffusion photovoltage. In contrast, there is no obvious relaxation peak for $ZnWO_4$ nanorods. Thus, it is reasonable to conclude that the presence of the interface between $ZnWO_4$ and Bi_2WO_6 can reduce the transfer rate of photoinduced charge carriers and inhibit the recombination of photoinduced charge carriers. In addition, the order of the diffusion photovoltage amplitude is 0.1 Bi_2WO_6/$ZnWO_4$ > 0.15 Bi_2WO_6/$ZnWO_4$ ≈ 0.05 Bi_2WO_6/$ZnWO_4$, suggesting that the extent of photoinduced charge separation induced by diffusion is the highest in 0.1 Bi_2WO_6/$ZnWO_4$ composite.

On the basis of the above data, it is believed that in the Bi_2WO_6/$ZnWO_4$ composite system, $ZnWO_4$ may supply photoinduced charges for the photocatalytic process, and the interface between Bi_2WO_6 and $ZnWO_4$ inhibits the recombination rate of photoinduced charge carriers. Because of the strongest TPV response and the largest retardation of the diffusion photovoltage, 0.1 Bi_2WO_6/$ZnWO_4$ composite possesses the effective separation of photoinduced electron−hole pairs and the low recombination rate of charge carriers, corresponding to its highest photocatalytic activity.

On the basis of the energy band diagram reported in previous literature[8,28] and band gap of $ZnWO_4$ estimated by us,[17] the

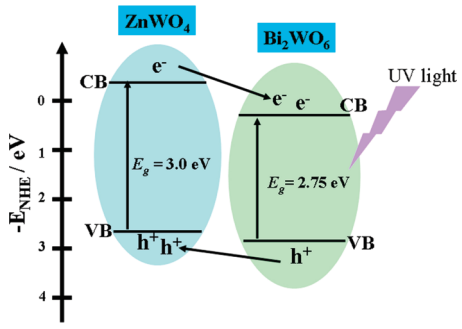

Figure 7. Band structure diagram and electron−hole separation of Bi_2WO_6/$ZnWO_4$ composite photocatalysts under UV irradiation.

calculated conduction band (CB) and valence band (VB) edge potentials of $ZnWO_4$ and Bi_2WO_6 are shown in Figure 7. Under UV irradiation, $ZnWO_4$ and Bi_2WO_6 would be excited simultaneously and generate electron−hole pairs. On the one hand, the CB-electrons ($ZnWO_4$) easily flow into the CB edge of Bi_2WO_6 through the interface because the CB edge of $ZnWO_4$ is higher than that of Bi_2WO_6. On the other hand, because the VB edge level of Bi_2WO_6 is lower than that of $ZnWO_4$, holes in the VB edge of Bi_2WO_6 will transfer to that of $ZnWO_4$ by the control of the interface. The results are consistent with the previous studies on the charge transition between semiconductor (such as TiO_2/Bi_2WO_6).[13,14] According to the TPV results, the photovoltage signals of samples appear on the time scale of milliseconds, which implies that the photoinduced electron−hole pairs are separated in space instead of the direct recombination between the VB edge and CB edge. As a result, VB holes with strong oxidation power can cast off from the pair recombination and be available to oxidize the pollutants, which supports the result that the Bi_2WO_6/$ZnWO_4$ composite exhibit higher photoctalytic activities than the pure $ZnWO_4$.

CONCLUSIONS

The Bi_2WO_6/$ZnWO_4$ composites were successfully synthesized by a simple hydrothermal method for the first time. The as-prepared Bi_2WO_6/$ZnWO_4$ composites are composed of Bi_2WO_6 nanoparticles grown on the primary $ZnWO_4$ nanorods. The composites exhibits enhanced photocatalytic activities in the degradation of RhB under UV light irradiation. When Bi_2WO_6/$ZnWO_4$ composites molar ratio is 0.1, the highest photocatalytic activity is observed. The enhanced activities of Bi_2WO_6/$ZnWO_4$ composites are attributed to the effective separation of photoinduced electron−hole pairs and the low recombination rate of charge carriers is due to the interfacial effect. The information provided here is expected to be useful for the further improvement of $ZnWO_4$ photocatalytic performances.

ASSOCIATED CONTENT

Supporting Information. Additional figures (PDF). This material is available free of charge via the Internet at http://pubs.acs.org.

AUTHOR INFORMATION

Corresponding Author
*Tel: +86 431 85168093. E-mail: xietf@jlu.edu.cn.

■ ACKNOWLEDGMENT

This work was supported by National Basic Research Program of China (973 Program) (2007CB613303), the National Natural Science Foundation of China (20703020, and 20873053), and the Science and Technology Developing Funding of Jilin Province (201115012).

■ REFERENCES

(1) Kudo, A.; Omori, K.; Kato, H. *J. Am. Chem. Soc.* **1999**, *121*, 1145.
(2) Asahi, R.; Morikawa, T.; Ohwaki, T.; Aoki, K.; Taga, Y. *Science* **2001**, *293*, 269.
(3) Zou, Z. G.; Ye, J. H.; Sayama, K.; Arakawa, H. *Nature* **2001**, *414*, 625.
(4) Fu, H. B.; Lin, J.; Zhang, L. W.; Zhu, Y. F. *Appl. Catal. A* **2006**, *306*, 58.
(5) Zhao, X.; Zhu, Y. F. *Environ. Sci. Technol.* **2006**, *40*, 3367.
(6) Lin, J.; Lin, J.; Zhu, Y. F. *Inorg. Chem.* **2007**, *46*, 8372.
(7) Huang, G. L.; Zhu, Y. F. *J. Phys. Chem. C* **2007**, *111*, 11952.
(8) Zhao, X.; Yao, W. Q.; Wu, Y.; Zhang, S. C.; Yang, H. P.; Zhu, Y. F. *J. Solid State Chem.* **2006**, *179*, 2562.
(9) Huang, G. L.; Zhang, C.; Zhu, Y. F. *J. Alloys Compd.* **2007**, *432*, 269.
(10) Zhao, W.; Song, X. Y.; Chen, G. Z.; Sun, S. X. *J. Mater. Sci.* **2009**, *44*, 3082.
(11) Yu, H.; Chen, M.; Philip, M. R.; Wang, S. X.; White, R. L.; Sun, S. H. *Nano Lett.* **2005**, *5*, 379.
(12) Bandara, J.; Hadapangoda, C. C.; Jayasekera, W. G. *Appl. Catal. B* **2004**, *50*, 83.
(13) Long, M.; Cai, W. M.; Cai, J.; Zhou, B. X.; Chai, X.; Wu, Y. *J. Phys. Chem. B* **2006**, *110*, 20211.
(14) Coló n, G.; Murcia Ló pez, S.; Hidalgo, M. C.; Navío, J. A. *Chem. Commun.* **2010**, *46*, 4809.
(15) Jang, J. S.; Li, W.; Oh, S. H.; Lee, J. S. *Chem. Phys. Lett.* **2006**, *425*, 278.
(16) Jang, J. S.; Kim, H. G.; Joshi, U. A.; Jang, J. W.; Lee, J. S. *Int. J. Hydrogen Energy* **2008**, *33*, 5975.
(17) Shang, M.; Wang, W. Z.; Zhang, L.; Sun, S. M.; Wang, L.; Zhou, L. *J. Phys. Chem. C* **2009**, *113*, 14727.
(18) Amano, F.; Nogami, K.; Abe, R.; Ohtani, B. *J. Phys. Chem. C* **2008**, *112*, 9320.
(19) Wei, X.; Xie, T. F.; Xu, D.; Zhao, Q. D.; Pang, S.; Wang, D. J. *Nanotechnology* **2008**, *19*, 275707.
(20) Peng, L. L.; Xie, T. F.; Lu, Y. C.; Fan, H. M.; Wang, D. J. *Phys. Chem. Chem. Phys.* **2010**, *12*, 8033.
(21) He, D. Q.; Zhang, X. R.; Xie, T. F.; Zhai, J. L.; Li, H. Y.; Chen, L. P.; Peng, L. L.; Zhang, Y.; Jiang, T. F. *Appl. Surf. Sci.* **2011**, *257*, 2327.
(22) Zhang, C.; Zhu, Y. F. *Chem. Mater.* **2005**, *17*, 3537.
(23) Dabbousi, B. O.; Rodriguez-Viejo, J.; Mikulec, F. V.; Heine, J. R.; Mattoussi, H.; Ober, R.; Jensen, K. F.; Bawendi, M. G. *J. Phys. Chem. B* **1997**, *101*, 9463.
(24) Zhang, Q.; Chen, X. Y.; Zhou, Y. X.; Zhang, G. B.; Yu, S. H. *J. Phys. Chem. C* **2007**, *111*, 3927.
(25) Timoshenko, V. Yu.; Duzhko, V.; Dittrich, Th. *Phys. Stat. Sol. (a)* **2000**, *182*, 227.
(26) Duzhko, V.; Timoshenko, V. Yu.; Koch, F.; Dittrich, Th. *Phys. Rev. B* **2001**, *64*, 075 204.
(27) Kronik, L.; Shapira, Y. *Surf. Sci. Rep.* **1999**, *37*, 1.
(28) Fu, H. B.; Zhang, L. W.; Yao, W. Q.; Zhu, Y. F. *Appl. Catal. B* **2006**, *66*, 100.